Oceanologia (2020) 62, 70—82

Available online at www.sciencedirect.com

ScienceDirect

journal homepage: www.journals.elsevier.com/oceanologia/

ORIGINAL RESEARCH ARTICLE

Dependence of acoustic noise emission on the dissipated energy of plunging waves

Zygmunt Klusek [a,*], Maciej Paprota [b], Wojciech Sulisz [b], Aneta Zdolska [b], Sebastian Sorek [b]

[a] *Institute of Oceanology, Polish Academy of Sciences, Sopot, Poland*
[b] *Institute of Hydro-Engineering, Polish Academy of Sciences, Gdańsk, Poland*

Received 13 December 2018; accepted 21 August 2019
Available online 6 September 2019

KEYWORDS
Wave breaking;
Wave energy dissipation;
Underwater noise

Summary The results of experiments performed in a wave flume designed to explore associations between the dissipation of surface wave energy during breaking and acoustic noise emission are presented. The experiments were carried out using tap water in the wave laboratory of the Institute of Hydro-Engineering of the Polish Academy of Sciences, Gdańsk, Poland. In particular, being shown are the parameters of empirical dependency between the dissipated wave energy during plunging and the energy of pre-breaking wave trains. Relationships between wave energy losses in the case of breakers with an amplitude of about 10 cm and the noise acoustic energy in the frequency band from 80 to 12,500 Hz were estimated. Taking into consideration the phenomena of reverberations and propagation in an acoustical waveguide, a numerical model was used for the correction of the observed noise's acoustic spectra. A detailed analysis of the factors affecting the noise level in the semi-enclosed volume allowed us to specify the rate of conversion of the wave energy dissipated during breaking into acoustic energy, which was found to be in the order of 10^{-8}.

* Corresponding author at: Institute of Oceanology, Polish Academy of Sciences, ul. Powstańców Warszawy 55, 81-712 Sopot, Poland. Tel.: +48 58 7311825. Fax: +48 58 551 21 30
E-mail address: klusek@iopan.gda.pl (Z. Klusek).
Peer review under the responsibility of Institute of Oceanology of the Polish Academy of Sciences.

https://doi.org/10.1016/j.oceano.2019.08.001

1. Introduction

When a wind wave is broken, a stream of water mixed with air is transferred into the water body.

To some extent, the energy of the pre-breaking wave is dissipated throughout this turbulent motion and doing work on newly created air bubbles by pushing them down. Despite great efforts, the present parametrisation of wave energy dissipation is far from completion.

Due to turbulence, clouds of mechanically agitated bubbles are formed. The bubbles are advected outwards from the breaking volume and upwards to the water surface, forming white caps. Plumes of aerated water are associated with emissions of wave-origin low-frequency (less than 1 kHz) ambient noise in the ocean (Carey and Browning, 1988; Carey and Fitzgerald, 1993; Prosperetti, 1988).

On the other hand, mechanically agitated individual bubbles ringing mainly at their radial resonance are a source of noise in the higher frequency range of up to tens of kilohertz (Medwin and Daniel, 1990; Prosperetti, 1988).

It is well recognised (for example, Kerman, 1984) that a predominant component of wind/wave-driven underwater noise exists in the ocean due to bubbles created throughout and immediately after wave breaking. Hence, it was observed that some functional dependency exists between dissipated wave energy in relation to the amount of acoustically active bubbles and emitted noise (Melville et al., 1988). Further, this idea has been put forward and tested (Lamarre and Melville, 1991), such that the intensity of underwater sound emitted during wave breaking correlates with the intensity of breakers and dissipation of wave energy.

Several laboratory and field experiments have supported the idea of associations between the character of wave breaking and some parameters of the emitted underwater noise (Deane, 1999; Deane and Stokes, 2010; Hollett, 1994; Kolaini,1998; Loewen and Melville, 1994; Means and Heitmeyer, 2001, 2002; Melville et al., 1993). Due to this relation, assessment of wind-wave energy dissipation in the ocean via measurements of the generated noise has been suggested, tested, and concluded that O (10^{-8}) of the dissipated wave energy is transformed into acoustic energy (Melville, Loewen and Lamarre, 1993).

However, observations performed on noise energy emitted during wave breaking contain a high degree of uncertainty concerning the rate of acoustic energy to the dissipated wave energy. The values differ by up to several orders of magnitude, ranging from 10^{-10} to 10^{-6} (Carey et al., 1993; Klusek and Lisimenka, 2013; Kolaini and Crum, 1994; Li and Farmer, 1993, 1994; Tęgowski, 2004). One of the reasons for this inconsistency concerns the different simulations of the wave breaking processes. On the other hand, as in the case of laboratory experiments, the distinctiveness of the sound propagation conditions in limited volumes was ignored.

Presented here experiment is one of the series of investigations designed to develop the relationships between breaking and noise at different scales of wave breaking intensities. In one of two earlier papers, the noise emitted by waves with a height exceeding 2 m was evaluated (Klusek and Lisimenka, 2013). In the other paper, it showed how salinity, microbubble presence and surface tension would influence sound generation during small-scale splash events (Szuszkiewicz and Klusek, 2018).

The motivation for this study is to determine more correctly the relations between energy dissipation of low amplitude waves (mainly plunged breakers) on the one hand, and the characteristics of emitted underwater noise aimed at monitoring breaking processes at sea on the other.

The paper is organised as follows. In Section 2, the wave flume and wave characteristics are briefly presented. Moreover, the acoustic setup, methods of signal recording and signal post-processing are there reported. Section 3 presents the parameters of acoustic noise, and in the next section, the acquired relationships between noise intensity and wave energy are presented and discussed. The paper ends with a discussion on the results obtained by some other authors.

2. Material and methods

2.1. Hydrodynamic investigations in the wave flume

The experiments were performed in a wave flume located at the Institute of Hydro-Engineering, Polish Academy of Sciences, Gdansk, Poland. The flume is 64 m long, 0.6 m wide, and 1.4 m high. The walls are made of 18 mm thick glass, which permits the application of imaging techniques of

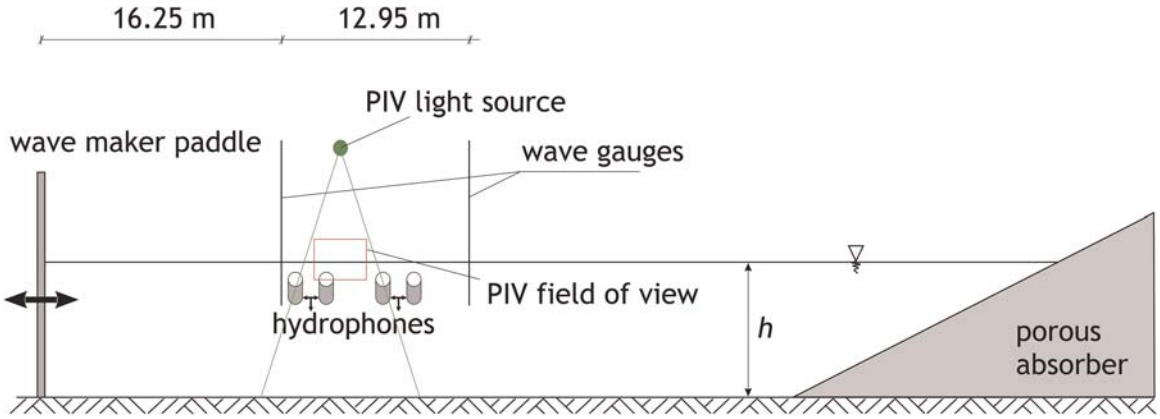

Figure 1 Wave flume setup and the arrangement of wave gauges and hydrophones.

measurements. The flume was filled with fresh water to a depth of 0.65 m. The temperature of water at the moment of the experiment varied between 14 and 16°C, depending on the date of the experiment.

In the hydraulic laboratory, waves are generated by a mechanical piston-type wave maker driven by an electric motor. The system's DHI Wave Synthesizer Online 8.1 software is used to control the generated sequences. At the far end of the flume, a porous wave absorber is installed to prevent wave reflections (Fig. 1).

The waves created and studied in the present experiments correspond to focusing wave packets comprising several component waves of fixed height and fixed wave period. The system is capable of creating both spilling and plunging breakers with various intensities. The maximum height of the generated waves may reach as high as 0.5 m. However, in the experiments, the maximum wave height usually does not exceed 0.3 m. Surface displacement is recorded with resistance type wave gauges placed in the prior- and post-breaking area, with a distance of 12.95 m between them (Fig. 1). Free-surface elevation time series are sampled at a frequency of 100 Hz. The gauges are calibrated before each experimental run.

In order to estimate the wave energy, the following spectral approach is applied. The free-surface elevation recordings are represented as the sum of harmonic wave components of frequency (ω_n), amplitude (A_n), and phase (φ_n) (Dean and Dalrymple, 1984; Goda, 2000):

$$\eta(t) = \sum_n A_n \cos(\omega_n t - \varphi_n), \tag{1}$$

where $\eta(t)$ is a function of free-surface elevation (displacement).

Applying Fourier analysis to the free-surface elevation time series, amplitudes of wave components (A_n) are determined. The wave energy of an individual component by a unit of the crest is calculated according to this equation (Dean and Dalrymple, 1984):

$$E_n = \frac{1}{2}\rho g A_n^2, \tag{2}$$

where g is the acceleration due to gravity and ρ is water density.

The total wave energy (E_T) of the wave packet is a sum of energies of individual wave components according to the formula

$$E_T = \frac{1}{2}\rho_w g l b \sum_n A_n^2, \tag{3}$$

where b is the width of the flume and l is the length of a wave packet.

The dissipation of wave energy may be estimated using the spectra of the two time series of the surface displacement taken before and after breaking. The lessening of wave energy after wave breaking event in relation to the initial wave energy would be presented in the form

$$C_d = \frac{E(x_1) - E(x_2)}{E(x_1)}, \tag{4}$$

where C_d is the dissipation coefficient, $E(x_1)$ is for the wave energy for the wave gauge positioned before wave breaking area, and $E(x_2)$ is for the wave gauge position behind the wave breaking area.

The coefficient C_d plays an important role in defining the intensity of the total energy dissipation.

In the course of some experiments, video recordings with a particle image velocimetry (PIV) system were performed, and the identification of bubbles' depth injection and behaviour was recorded. The 2D FlowMaster software from LaVision was used. The PIV system comprises a high-speed CCD camera with a resolution of 1280 × 1024 pixels and Nd: YAG 200 mJ dual laser-head system (described as PIV light source in Fig. 1). The system allows for collecting images in memory at a 15 Hz sampling rate. The measurements were performed in a plane parallel to the wave flume walls (described as PIV field of view in Fig. 1). The PIV camera records the movement of air bubbles illuminated by laser light in the selected field of view. The impulse of a laser light 'freezes' the moving air bubbles in a few mm thick layer, parallel to the wave flume walls. The laser and the camera measurement system is capable of providing high-quality data for the computation of air bubbles' displacement based on the identification of the bubble position in two successive images taken within a very short time span between them (~1 ms). The recorded raw images are then post-processed using a PIV double frame – double exposure method. This technique implicates the calculation of vector velocity fields based on a spatial cross-correlation between two images (Paprota, 2017). The 2D cross-correlation method is applied to a number of smaller windows (32 × 32 pixels) that cover the entire field of view and allow for visualising the spatial mean displacement of illuminated bubbles distribution within the whole window. Finally, the vector of instantaneous velocity between two camera exposures is calculated. This procedure is repeated 15 times per second to capture the temporal evolution of fields of the bubble velocity vector in the course of the breaking event.

2.2. Hydrodynamics data processing

The generated wave packets were focused at a distance of around 20–22 m away from the mean position of the wave maker paddle. As soon as the wave's steepness exceeds a certain critical value of the wave-breaking criterion, a plunging breaker or spiller occurs. The maximum recorded wave height upstream of the breaking point was about 0.2 m. The particular run was repeated 3 times for each of the selected wave energy. In total, 103 runs were performed, including 12 spilling breaker events generated for different wave energy packets. However, due to the fact that the experiments were carried out in different seasons at slightly different water temperatures (14°C in wintertime and 19°C in summertime), only a subsample of 48 runs from the experiments in the winter season was used in this analysis.

In Fig. 2, examples of wave sequences initiating spilling (top graphs) and plunging (bottom graphs) breakers are presented in terms of the free-surface elevation records and corresponding spectra of relative wave energy (normalised by the specific weight $\gamma = g\rho$). The elevations measured by the upstream gauge are denoted in black, while downstream ones are denoted in blue.

In the example presented, the wave sequence leading to the plunging breaker comprises waves in a frequency ranging from 0.2 to 1 Hz, while the spilling breaker occurs in a

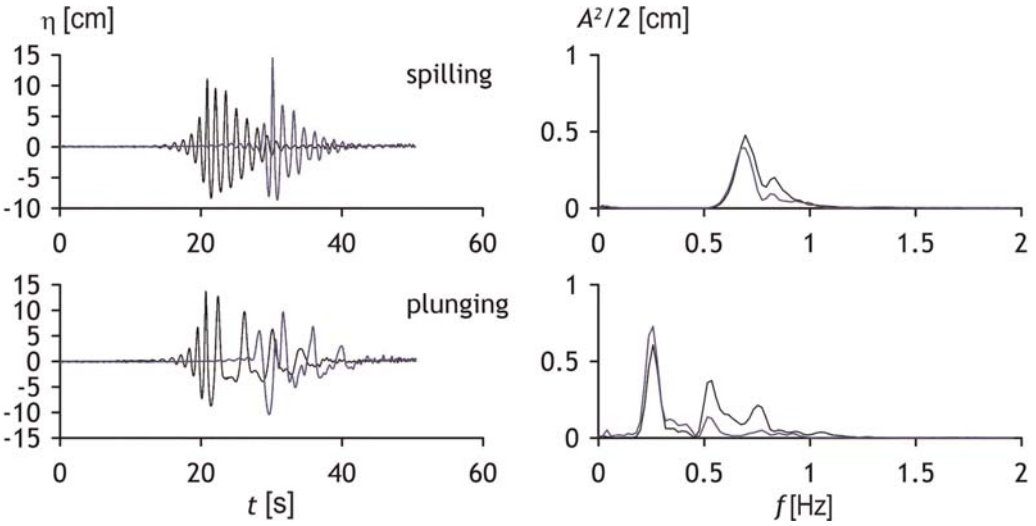

Figure 2 Free-surface elevation time series and corresponding wave energy spectra before (black) and after (blue) the occurrence of a spilling breaker (top); plunging breaker (bottom). (For interpretation of the references to color in this figure legend, the reader is referred to the web version of this article.)

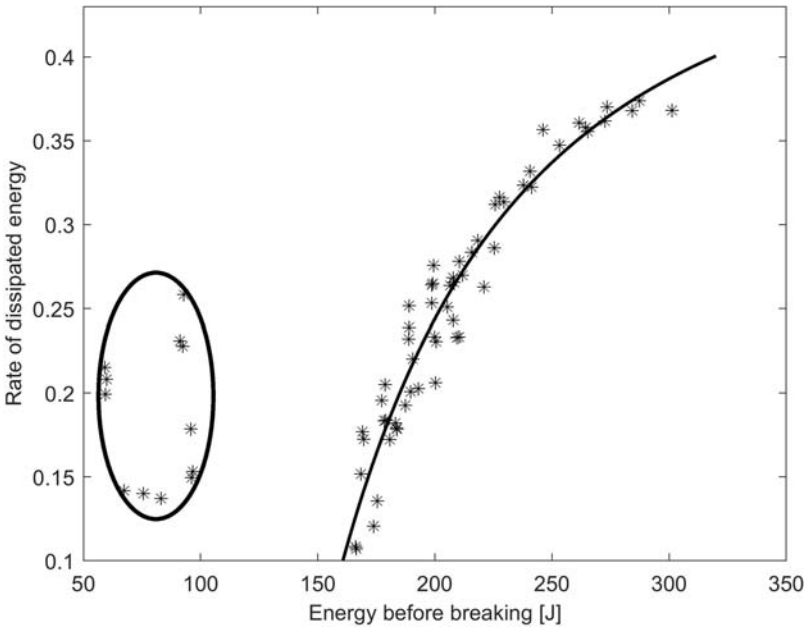

Figure 3 Energy of wave packets before breaking and dissipation rates of energy as a function of initial wave packet energy. The best fitted curve is proposed in the form $C_d \sim E_{T1}^{-1.69}$, where T1 — the energy of a wave packet before breaking. The set of spiller events is inside the ellipse.

narrower frequency ranging from 0.5 to 1 Hz. The spilling process usually occurs in the case of less energetic wave packets when compared to plungers.

The way in which the dissipation coefficient C_d relates to the pre-breaking wave energy suggests that possible dependency is in the form of power-law function.

Fig. 3 demonstrates a more rapid increment in the lowest range of the investigated energy of plungers than in the middle of the scale, and furthermore the gradual decrease in the growth rate at the end of the scale. The latter is probably due to the saturation of the dissipation process.

The relationship is proposed in the form of:

$$C_d = \frac{\Delta E}{E(x_1)} = a \cdot E(x_1)^b + c, \tag{5}$$

where the exponent is $b = -1.69$ and the adjusted R-square value is 0.99.

The observed rate of dissipated energy is growing from about 10% for the less energetic waves, and at up to about 37% in the largest breaking (Fig. 3).

Dissipation rates for spillers, which are marked with an ellipse, show rather random differences depending on the

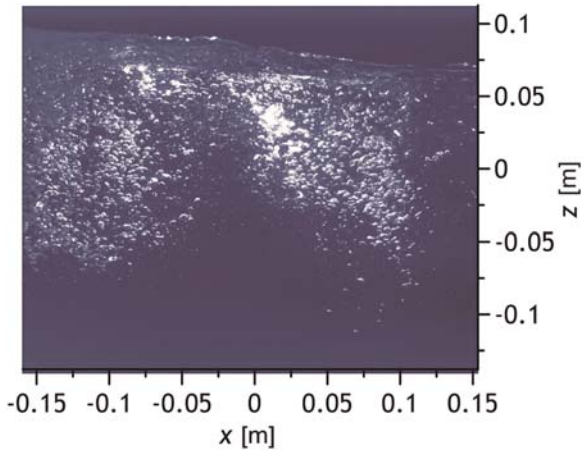

Figure 4 The PIV camera image of air bubbles under a plunging breaker.

wave character, and are noticeably distinguished between the similar spilling events. Additionally, higher energy dissipation is observed for higher energies of the wave trains.

At the next stage, the dynamics of air bubbles produced during the breaking events were determined qualitatively. In Fig. 4, the recorded camera image of the illuminated air bubbles, allowing for the determination of bubble kinematics, is presented.

Comparing different runs, we observe the entrainment depth of bubbles as rather regular which is approx. in the range of 0.12—0.15 m. The horizontal length of the bubble plume stays within a range of 0.2—0.4 m depending on the breaker intensity.

Fig. 5 illustrates the velocity field of bubbles for the case of the generated wave train consisting of several component waves of periods ranging from 1.0 s to 5.6 s with the corresponding wavelength ranging between 1.6 and 14 m. The estimated minimum and maximum phase celerity of component waves is 1.6 m/s^{-1} and 2.5 m/s^{-1}, respectively. It can be seen from Fig. 5 that the air bubble velocity field reveals a dynamic and complex nature of wave breaking phenomenon. In the example presented, the highest bubble velocities may reach 3.2 m/s, which constitute approximately 130% of the highest phase celerity, thus corresponding to the longest component wave.

Although laboratory conditions do not fully reproduce the situations in the sea, bubble plumes formed by plunging waves and the waves themselves may be easily reproduced and carefully controlled, thus allowing hydrodynamic and acoustic parameters to be investigated quantitatively.

In numerous studies, a lot of attention was paid to the issue of how salinity affects the number of created bubbles (Anguelova and Huq, 2018; Blenkinsopp and Chaplin, 2007, 2011; Cartmill and Su, 1993; Chanson, Aoki and Hoque, 2006; Haines and Johnson, 1995; Kolaini, Roy and Gardner, 1994; Orris and Nicholas, 2000; Slauenwhite and Johnson, 1999; Wu, 2000). To date, the interpretations have been contradictory. However, comprehensive research conducted by Blenkinsopp and Chaplin (2011) shows that the number of very small bubbles inside a breaking-induced plume in seawater is greater than that in fresh water even though

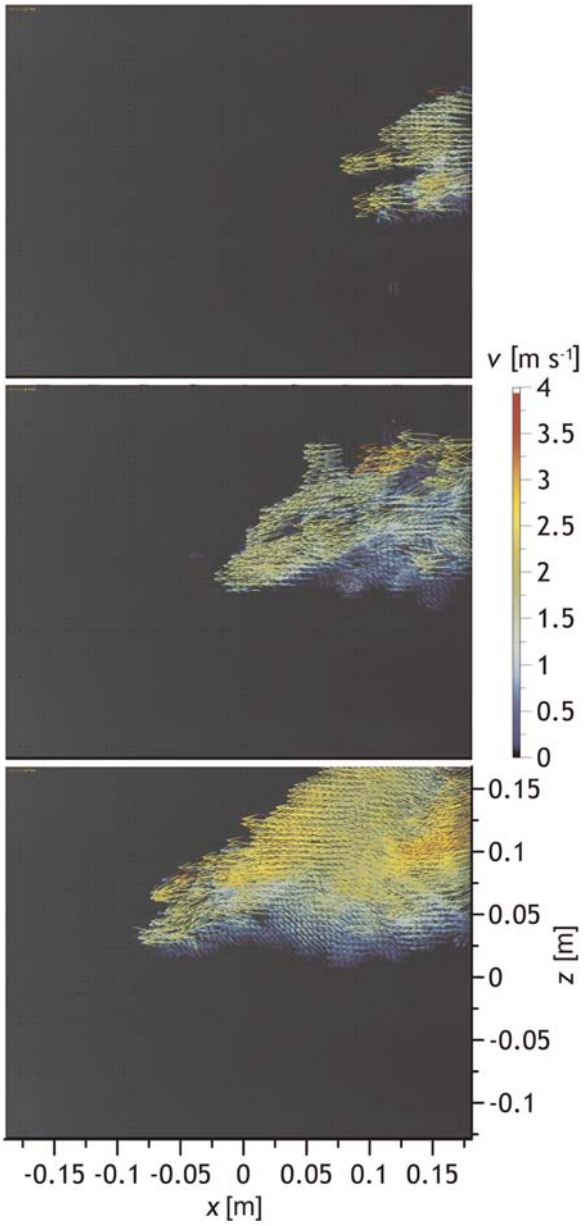

Figure 5 The velocity field of air bubbles produced by a plunging breaker. The images represent subsequent instants of a wave breaking process recorded every 1/15 s.

the overall differences in air entrainment and bubble size distribution are negligible.

2.3. Underwater noise recordings

Noise recordings were realised using a setup of four omnidirectional hydrophones spaced horizontally along the flume axis. The hydrophones were grouped pairwise, with a distance inside each pair of 65 cm, positioned midway between the walls and 25—30 cm beneath the still water surface. In the case of plungers, one pair of hydrophones was placed upstream and another downstream of the breaking area at a distance of 6.1 m between the group's centres. In the case of

spillers, the location of the array of hydrophones was extended under the whole spilling area.

The transducers were broadband RESON TC 4032 hydrophones calibrated by the manufacturer.

For some runs, rubber sheets were attached to the bottom and to the walls of the flume to diminish reverberations of the acoustic waves. The tests showed that the sheets insignificantly affect acoustic observations. But then, the dynamics of breaking waves were disturbed when compared to the conditions without the sheets. Consequently, presented here are the results of the experiments devoid of any additional attachments aimed at reducing reverberations.

The acoustic signal was acquired using a 16-bit resolution National Instrument 6251 Analog Digital Converter and further analysed using specially designed (and developed by the authors) software in the MATLAB environment.

The sampling rates in each of the four channels started at 50 Ksamples/s, and in one of the series, they increased to 70 Ksamples/s. The low- and high-pass analogue filters were set at the amplifier with a bandwidth in the range of 100 Hz to 25 kHz.

To estimate the duration of the noise generated by the active bubbles, the information at the level of the background noise of the tank was taken into account. High-resolution power spectra were calculated by means of the sliding FFT algorithm operating on 8192 long sub-samples with a rectangular window. One-third octave frequency band spectra were calculated at the outcome set of the narrow-band spectrum as the mean of frequency power component in a given frequency band.

2.4. Adjustment of acoustic data in view of propagation in waveguide

The advantages of tests in a flume are well known and are mainly due to performing the experiments under strongly controlled wave conditions, such as their spectra and energy. Furthermore, the geometry of experiments could be designed and it is possible to repeat them.

Nevertheless, in the field of acoustics, we face major environmental challenges such as signal contamination by ambient noise in laboratories and the surrounding area, and wave-maker sounds and strong reverberation in small tanks. The other disadvantage is that due to proportions of the cross-section of the acoustic waveguide in relation to the wavelength in the investigated range of frequencies, the cut-off frequency phenomenon in the middle range of audio frequencies is observed, and requires the use of data correction algorithms.

Moreover, as was mentioned above, the difference compared to the seawater physicochemical properties of tap water regularly utilised in tanks, i.e. salinity, surface tension or presence of microbubbles might change noise emission.

From an acoustic standpoint, the flume would be regarded as a waveguide with rectangular cross-section enlarged in one dimension.

In such cases of enclosures, the method of images would be applied in the frame of the geometrical acoustics approximation (ray acoustics) (Allen and Berkley, 1979; Gibbs and Jones, 1972), while the concept of a sound wave is replaced by the concept of sound rays.

However, for boundaries that have a finite admittance, only an approximate solution for the pressure can be obtained (Ingard, 1951). Formally, the correct solutions are obtained in the case where the distances of both the source and observation point are greater than a quarter of the acoustic wavelength from the wall. Nonetheless, as stated by Deane and Stokes (2010), the method of image yields a reasonable approximation of the observed noise spectra in a size similar to a flume.

However, our modelling research, performed with the method of images, satisfies recorded spectra only at small distances between the source and receiver.

Using the method of images for a point source, the sum of pulses can be expressed as:

$$h(t,\vec{x}_S,\vec{x}_r) = \frac{\delta(t-R_0/c)}{R_0} + \frac{\delta(t-R_B/c)}{R_B}\tilde{V}_B + \frac{\delta(t-R_S/c)}{R_S}V_S + \frac{\delta(t-R_{W1}/c)}{R_{W1}}\tilde{V}_B + \ldots\frac{\delta(t-R_{W2}/c)}{R_{W2}}\tilde{V}_B + \frac{\delta(t-R_{BS}/c)}{R_{BS}}\tilde{V}_B V_S + \frac{\delta(t-R_{W1S}/c)}{R_{W1S}}\tilde{V}_B V_S + \cdots, \quad (6)$$

where R is the length of a sound path from a source to the receiver bouncing at the bottom, sidewalls and water surface; for example, R_{BS} means the path between a source and the receiver reflected once at the flume bottom and once at the water surface.

$\tilde{V}[\ldots]$ are the complex reflection coefficients at the boundaries, respectively at the water surface and flume walls or bottom, depending on the frequency and angle of incidence. In view of the fact that the sidewalls and bottom of the flume are the same, we have $V_{w1} = V_{w2} = V_B$.

δ is the Dirac delta-function which generates a peak in an impulse response (IR) at arrival time $t = R/c$.

For the estimation of interactions at each boundary, the angle of incidence is computed and the reflection coefficient from a water-glass-air sandwich-type layer is modelled by the frequency and angle independent of reflection coefficients with the standard formula according to Brekhovskikh and Godin (Brekhovskikh and Godin, 1990, formula 2.4.9):

$$V = \frac{(Z_1+Z_2)(Z_2+Z_3)\exp(-2i\varphi) + (Z_1-Z_2)(Z_2+Z_3)}{(Z_1-Z_2)(Z_2+Z_3)\exp(-2i\varphi) + (Z_1-Z_2)(Z_2-Z_3)}, \quad (7)$$

where Z_1, Z_2, Z_3 are respectively the acoustic impedance of air, glass, and water; while the acoustic impedance of a medium is $Z = \rho c$, where ρ is the medium density and c is the sound speed in each of the media.

$\varphi = 2\times k_2 d\cos\theta_2$, and k_2 is the acoustic wave number in the glass layer, θ_2 is the angle of refraction in the glass, and $d = 0.018$ m is the thickness of the flume walls.

In order to calculate the acoustic impedance, densities and sound speeds in the media were applied as follows:

water $\rho = 999.8$ kg/m^3, $c = 1470$ m/s;
glass $\rho = 2500$ kg/m^3, $c = 4500$ m/s;
air $\rho = 1.2$ kg/m^3, $c = 343$ m/s.

In the considered frequency range below 12 kHz, the reflection coefficient from the flume walls is complex, with the absolute value close to unity and is practically not dependent on frequency and incident angle. In contrast, the phase shift of reflected waves depends, in a smooth

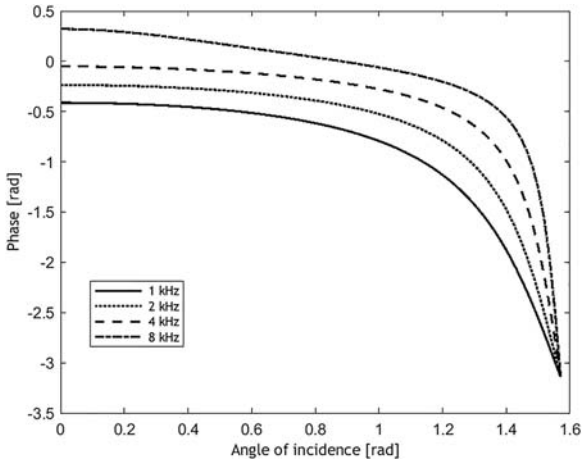

Figure 6 The dependence of the phase shift of reflected waves from the flume's walls upon frequency and incident angle.

manner, on the frequency and incident-reflected angle and at higher frequencies above 10 kHz in a rather complicated one (Fig. 6).

To determine the amplification of sound level at some frequencies and attenuation in another frequency band due to wave propagation in the limited volume of the flume, the reverberation was initially computed as the incoherent sum of the sound pressure at each of the receiver locations. And, subsequently, the incoherent sum of the sound pressure was normalised by the sound pressure in the absence of reverberation. It means that the sum of terms in Eq. (5), multiplied by noise in some frequency band and divided by the first term, gives a series of normalisation coefficients used for the correction of the observed power noise spectra.

The numerical tests were taken by planting a number of point sources near the duct's surface which corresponds to bubbles dispersed in the volume of the size of images of bubble clouds recorded by the camera.

In the model, the receivers were placed along the flume axis. The generated signals were white noise time series filtered in one-sixth octave bands.

Illustrations of the behaviour of spectra for a discrete set of frequencies corresponding to steps with the 1/6 octave-bands in the 80—12,500 Hz range at different distances from sources are given in Fig. 7.

After running tens of realisations, correction (compensation) for the observed sound spectra and acoustic energy in 1/6 octave bands emitted during the plunging was carried out.

Due to the relatively small dimensions of the flume's cross-section in relation to acoustic wavelengths in the middle of the audio frequency band, the cut-off phenomenon is observed. Hence, strengthening or reducing the sound intensity, which depends on the frequency and distance of the observation point to the source, is evident.

In the illustrated example, a number of point sources n are equal to 300. The sources are uniformly and randomly distributed between the walls of the flume, in the water column from the mean water surface down to $d/4$, and along the flume at a distance of up to 0.2 m. Here, the points of observations are situated in the centre of the flume's cross-section at distances of 0.5, 1, 1.5, 2.0 and 1.5 m from the front edge of a bubble cloud. As was shown by Deane (1999), the sound attenuation in an air-water mixture under the breaking wave would reach tens of dB/m, so the noise recorded outside of the mixed area is coming from a relatively thin “skin” of bubble cloud.

3. Results

3.1. Characteristic features of the noise

High-resolution periodograms of plunging noise, recorded by each of the hydrophones, and estimated with the short-time Fourier transform (STFT), are given in Fig. 8.

The spectra of signals received at each of the hydrophones, arranged along the flume at different locations in

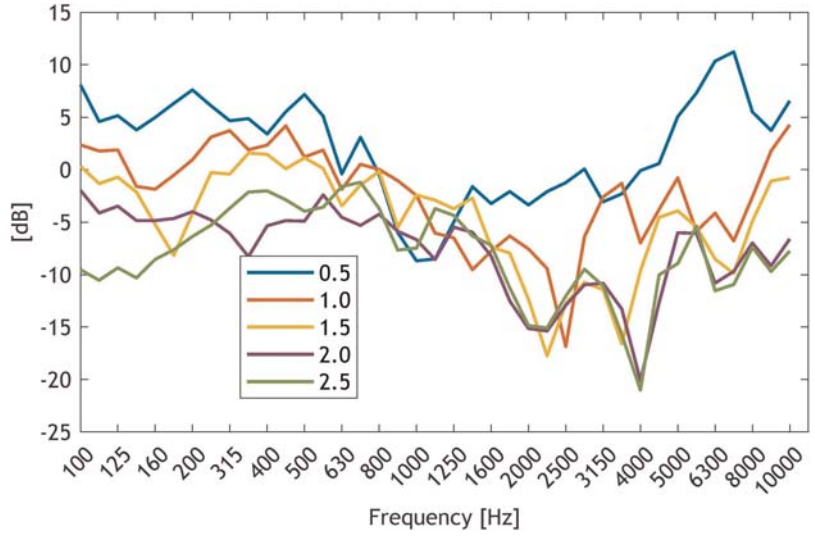

Figure 7 Normalised, spectral characteristics of reverberation, computed from the model for the set of frequencies in 1/6th octave bands ranging from 80 to 12,500 Hz. Hydrophones are placed in the geometrical centre of the water column's cross-section. Numbers in the legend are for hydrophones placed at distances of 0.5, 1, 1.5, 2 and 2.5 m from the edge of volume with bubbles.

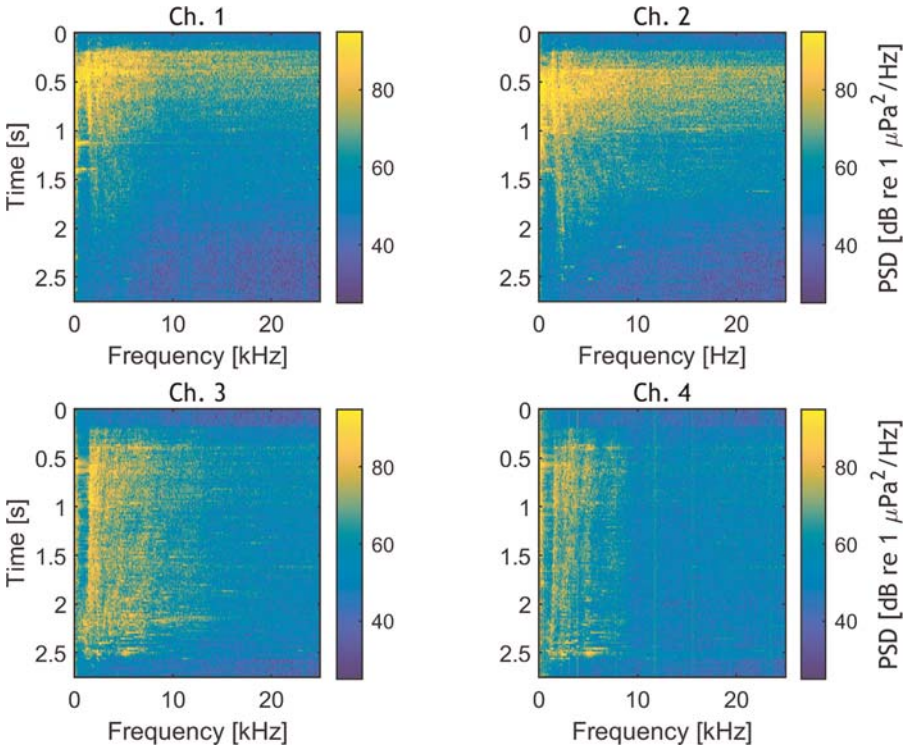

Figure 8 Examples of time evolution of the noise power spectrum in narrow frequency bands during the course of breaking, registered by all the hydrophones. The example illustrates one of the most energetic events. Colours represent the Power Spectral Density Level of the noise. (For interpretation of the references to color in this figure legend, the reader is referred to the web version of this article.)

relation to the breaking area, are presented in subsequent panels. The upper panel is for data from the hydrophone situated at the most distant point, which is upstream in relation to the breaking area. Each periodogram presents an evolution in time of noise radiation at different stages of the breaking process. Additionally, the effects of the modal broadband sound propagation on the acoustic waveguide in the case of a source moving in relation to the observer are observable. Subsequently, for frequencies above the lowest in the set of cut-off frequencies, the interference pattern predicted by the wave theory of guided waves is evident.

The plunging event shown here is relatively fast, with the highest sound emission lasting only 1.5—2.5 s.

In the middle of the audio frequencies' range, and going down in line with the frequency axis, we observe a notch with a sharp decline in the noise spectra. It corresponds to the lowest cut-off frequency (which matches the length of acoustic wave equalling four of the water depths in the flume). When an acoustic active volume drifts off from a receiver, the increasing mode number of the cut-off frequency also increases. We observe that at frequencies approximately below 1600 Hz, due to the excessive attenuation, the noise intensity decreases exponentially with the increasing distance to a source. At further distances from the breaking area and in the lowest frequency range, only plane waves would propagate.

On the other hand, in the vicinity of a bubble cloud, both the acoustic properties of the flume walls and its geometry do not have much influence on the noise spectrum.

Examples of the evolution of noise spectral density for the duration of breaking in 1/6-octave bands, registered at two hydrophones, are shown in Fig. 9.

It is evident in the time history of noise in selected frequency bands that at the hydrophone situated upstream from the breaking region (the upper panel, Channel 2), the noise level at the lowest observed frequencies increases at the very moment that the breaking happens. We believe that at this moment the noise is emitted simultaneously by single bubbles and by the first produced bubble cloud.

Generally, in the course of the first half-second of the rolling, the central frequency displays a shift towards higher frequencies and is correlated with changes in the spectral slope.

The active generation of the sound after plunging depends on the wave intensity, and in our experiments, it lasts up to about 3 s. The noise intensity decayed exponentially in time, and in the first 1—2 s after maximum, the intensity diminishes by a factor $-6 \div -10$ dB/s.

The mean noise spectra are reasonably similar for all wave heights. The negative slope of the spectrum envelope above 1.5 kHz is about $-6 \div -10$ dB/octave, reaching the minimum in the first second of breaking.

It is understandable that in the tank, the noise intensity should be higher due to multiple reflections from the water surface, tank bottom and walls, and at the same distance from the breaking area as in boundless space. Therefore, the real spectral slope and total sound energy emitted during a breaking event at the source would be obtained using

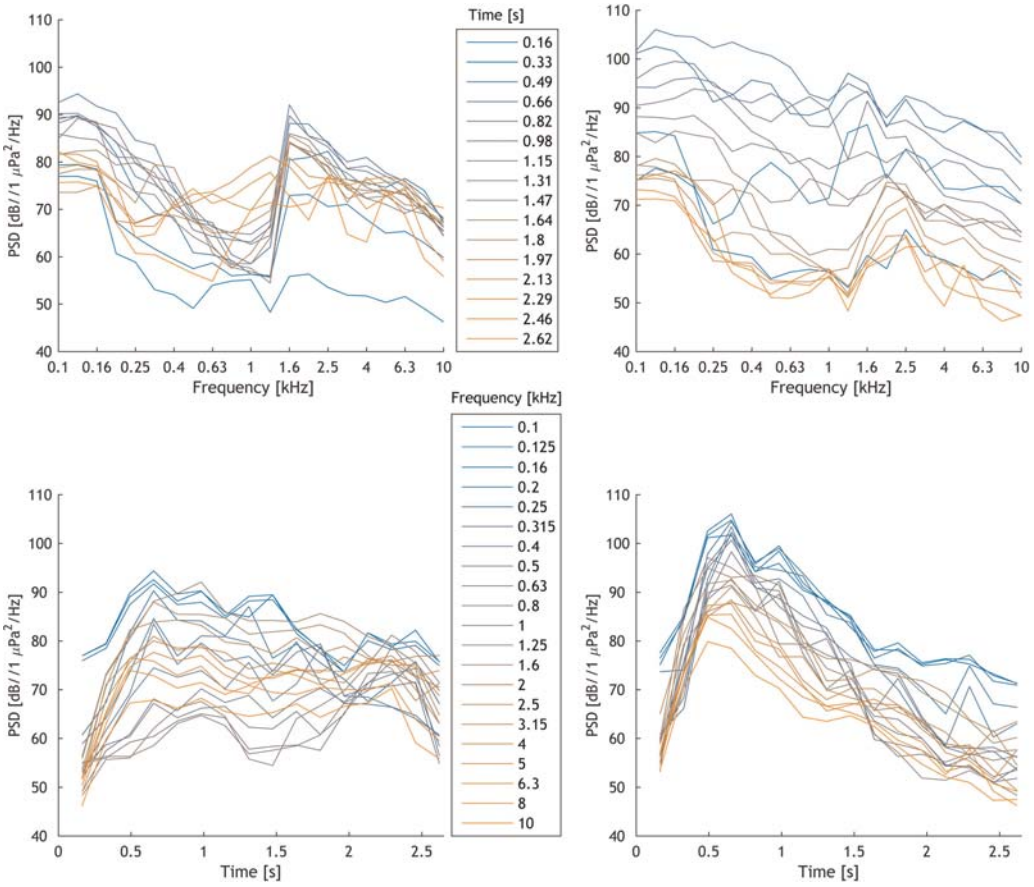

Figure 9 The time history of unprocessed noise signals recorded by the two hydrophones observed at different frequencies (upper panels). The receivers are placed upstream (Ch.2) and downstream (Ch.3) in relation to a plunger in the vicinity of the breaking area. Numbers in legends are central frequencies in 1/3-octave bands. The bottom panels are spectra at different moments of the breaking process. Numbers in the legends represent time in seconds.

correction for the spectra of signals received at different hydrophones.

With the model results, we would then correct the received sound spectra. The appropriateness of doing this kind of adjustment is confirmed by comparing the observed slope of the noise spectra in the flume with the noise spectra from plungers in the sea, which have similar typical values of −5 to −6 dB/octave. However, when introducing adjustment to the noise spectra attributable to reverberation and excessive attenuation, the notch at the middle of the spectra is corrected though only to some extent.

3.2. Estimating the energy of the emitted noise

As a consequence of the extent of the sound generation volume in relation to the channel cross-section, and due to small distances from a set of sources to an observation point, estimation of the total source intensity with the application of the model of dipole point source placed in a boundless medium (as among others by Kolaini and Crum, 1994 or Tęgowski, 2004) is not appropriate here. At the observation point located outside of the breaking area, noise is coming from different directions due to multiple reflections. On the other hand, at higher distances in the lower frequency range, only plane waves do arrive. In general, both effects are predicted by the theory of sound propagation in an enclosed space, though only for an idealised case of propagation in a medium with uniform acoustic properties.

The estimation of the sound energy generated in a single breaking is carried out under the following steps:

- estimation of the power spectrum in the third-octave bands for 8192 points sampled at 50 or 70 kHz;
- multiplying the spectral values of energy of raw recorded signals in each of the third-octave bands by appropriate weights resulting from amplification or weakening of the signal in different frequency bands (based on smoothed data from Fig. 7);
- summing up over frequency and time;
- and at the last stage, acoustic energy transferred through the flume's cross-section is computed.

The released acoustic energy in the course of breaking events at each observation point would be performed according to the following formula:

$$\prod = \frac{s}{\rho_w c_w} \sum_{i}^{n} \sum_{j}^{m} w_{ij} \langle P_{j,k}^2 \rangle df_i dt, \tag{8}$$

where ρ_w is the water density [kg/m^3], c_w is the sound speed in water [m/s], n is the number of one-third octave bands, m

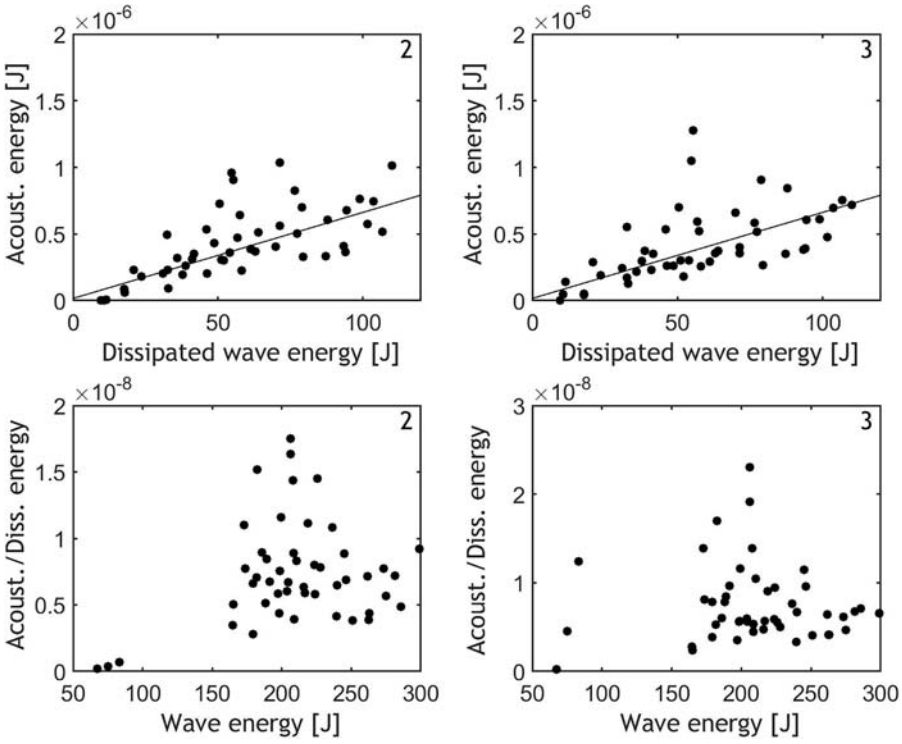

Figure 10 Rate of emitted acoustic energy to wave energy dissipated during breaking events estimated at selected observation points as functions of the dissipated wave energy (upper panels) and the wave packet energy before breaking (bottom panels). In the panels, numbers of hydrophones represent their positions along the flume.

is the number of segments taken into instantaneous spectral analysis, $\langle P_{j,k} \rangle$ is the mean acoustic pressure in frequency band and each of segment [Pa], df_i is the frequency range in each of one-third octave bands, w_{ij} is the correction coefficients for each frequency band and distance from a bubble cloud to a hydrophone, and s is the cross-section of the flume's water body.

3.3. Energy of the emitted noise vs. dissipation of wave energy

The rate between the emitted acoustic energy and the wave energy dissipated during breaking as well as the wave energy predating breaking is demonstrated in Fig. 10. The hydrophones are numbered as in Fig. 8; numbers 1 and 3 are for hydrophones placed afterwards (hydrophone No. 3) and in advance of the breaking area (hydrophone No. 1). The lines in the upper panels denote tendency towards increasing acoustic emission with the dissipated wave energy. Fitting was performed with the robust nonlinear methods using "bisquare" weights (MATLAB) to diminish the effects of accidental data points, which do not follow the general trend in other observations.

Some effects are evident: firstly, there is increased efficiency in the conversion of dissipated wave energy into acoustic energy with increasing losses of wave energy; secondly, emission in the direction of the wave propagation is higher as from the rear of a bubble cloud. The latter effect supports the hypothesis that noise is predominantly emitted in the direction of wave propagation, i.e. at the front edge of rollers. Comparing the upper and bottom panels, it is also clearly visible and distinctive that noise emission is more orderly dependent on energy dissipation than on wave energy.

Observations of the time-frequency behaviour of noise and then comparing them to the results from the model indicate that the sound energy at frequencies greater than the cut-off frequency varied less than in the lower frequency range. Additionally, in this frequency range, due to the acoustic waveguide geometry, the sound is less excessively attenuated in the flume, and the noise level is generally more predictable than at lower frequencies. Besides, within a frequency range between 1 and 8 kHz at the sea, we observe the highest correlation between noise and wind speed (Klusek and Lisimenka, 2007, for example), which means stronger interrelations between the noise intensity and intensity of wave breaking, and associated with this is the dissipation of wave energy.

Consequently, to diminish the impreciseness of the adopted model for the spectrum correction, the energy of the high-frequency component of noise as a measure of the integrated total noise estimation has been proposed. The cumulative noise level in the frequency band (f, $f + df$) over a given time of emission is defined as:

$$CNL(f, f+df) = 10 \log \frac{\int_0^T p^2(f, f+df, t)dt}{p_0^2}, \quad (9)$$

where CNL is the cumulative noise level, f is the acoustic frequency of interest, df is the width of the frequency band, and t is time.

The relationship between a cumulative noise level in one of the higher frequency bands and dissipated wave packet

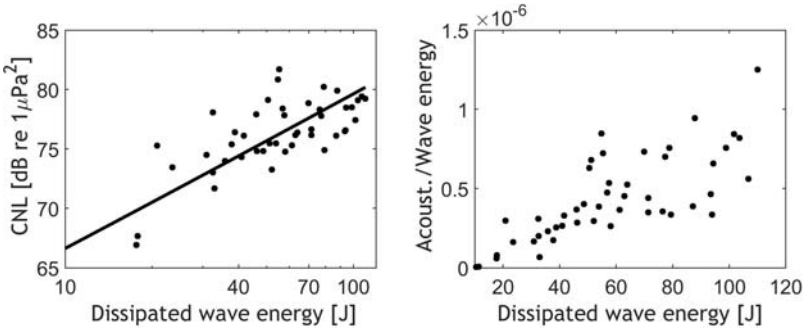

Figure 11 Cumulative noise level emitted during breaking events in 1/3rd octave band with a central frequency of 5 kHz, as a function of dissipated wave energy (on the left) and projected on the basis of this noise energy in broad frequency range (on the right). Presented data are recorded by the hydrophone 3 placed downstream of the breaking area.

energy during breaking is shown in Fig. 11. The noise data are only in the one-third octave band, with a central frequency of 5 kHz. Noise is recorded on the hydrophone placed downstream, in the vicinity of the acoustically active water volume.

Data are then fitted by means of the least square method using equally weighting data with a linear relation between decimal logarithm of dissipated wave energy during breaking and cumulative noise level.

$$CNL(@5\,\mathrm{kHz}) = p_1 \log_{10}(\Delta E_n) + p_2, \tag{10}$$

where the estimated value of p_1 is 11.12, meaning that we have the approximately linear relation between the level of acoustic energy at higher frequencies and the logarithm of dissipated wave energy (expressed in dB).

There are experimentally well-documented facts, verified on large datasets, that the acoustic radiation from the turbulent volume of a water-air mixture under plunge breakers both at sea in a coastal zone by Bass and Hay (1997) or in a laboratory (Kolaini and Crum, 1994) has some universal properties. The broad maximum in noise spectra is placed within a range of 500—800 Hz; in addition, within a range of 1 to 10/20 kHz the slope of the spectral envelope is reasonably repeatable and has a negative roll-off rate of −5 to −6 dB/octave.

Hence, in principle, we can deduce the noise energy emitted during breaking in a broader frequency range via extrapolation and integrating noise spectra towards lower and higher frequencies from the frequency band presented here.

The results of interpolation of the PSD, with the straight line passing through the point of the noise level at 5 kHz, down to 500 Hz and up to 12,500 Hz (with a spectrum slope of −6 dB/octave) gives similar results for the ratio of energy conversion as using measurements in broad frequency band.

As a result, on the basis of the experiments presented, we would state that the ratio of the emitted acoustic energy to the mechanical energy of the waves dissipated in the plunging is in the order of 10^{-8} which coheres with the results of other investigations (Klusek and Lisimenka, 2013).

4. Discussion

In this section, our results are compared with the existing research on the relations between the emitted acoustic energy and wave energy dissipation that are either observed in the field or simulated. The experiments have different objectives and approaches but are nonetheless representative of a broad range of wave energy, hence the intensity of breaking.

In laboratory experiments, Loewen and Melville (1994) showed that the acoustic energy generated by a breaking wave was increasing with the wave energy dissipated by the breaking event. They estimated that the ratio of acoustically radiated energy to the energy dissipated by the breaking wave was O (10^{-8}).

Kennedy (1992, 1993) estimated that the ocean acoustic energy radiated during breaking comprised between 10^{-6} (Kennedy, 1992) and later after some correction 10^{-8} (Kennedy, 1993) of the dissipated wave energy.

Carey et al. (1993) simulated wave breaking with a wedge by releasing salt or freshwater into a semi-enclosed submerged rubber bag. Pouring was performed from different heights — from 0.34 to 0.9 m above the water surface. It was meant to imitate breaking waves with various potential energy. The experiments were conducted in a deep lake, and acoustic records were performed in the far field with respect to the noise source in the environment without reverberations.

The efficiency of the process of converting water energy to acoustic energy was within a range of 0.3—2.3×10^{-8}. Generally, they found 5-times lower acoustic energy emitted in the case of saltwater compared to a freshwater environment.

Kolaini and Crum (1994) performed an experiment using a set of wave packets with potential wave energy between 4 and 11.5 J. They observed both spillers and plungers events, and found different relations between the radiated noise energy and the energy of surface waves. The acoustic energy was rising more steeply in the case of higher energies of breakers, and sloping or just lacking any functional relationship for spillers (Fig. 11 in Kolaini and Crum, 1994). The latter observations have been supported by the measurements presented here.

The acoustic records were performed in an anechoic tank. The ratio between the emitted acoustic energy and potential energy of the wave before breaking was estimated within a relatively narrow range of 0.8×10^{-7} to 1.09×10^{-6}, with a higher conversion rate in the case of “stronger” waves.

When converting the results of Kolaini and Crum according to the convention adopted in our work regarding the ratio of the acoustic energy to the wave energy dissipated during breaking, and assuming the value of the dissipation coefficient to be $C_d = 0.1$, the transformation of the dissipated wave energy to acoustic energy is from 0.8×10^{-8} to 1.09×10^{-7}.

The ratio of the acoustic energy generated by breaking waves to the energy dissipated in breaking waves was estimated by Tęgowski (2004) in the Ocean Basin Laboratory at MARINTEK, Trondheim, Norway. The 3D-sea wave spectra were reproduced in a more realistic way than in 2D the wave flumes. The efficiency of transformation of the dissipated wave energy into acoustic energy with amplitudes in the order of 10 cm was found to vary within a range of 1.0×10^{-7} to 4.1×10^{-7}. However, in the estimations, the author disregarded the multiple sound reflections between the bottom and water surface, therefore the results might well be overestimated. Also, due to the fact that the waves were not in the form of packets, the author did not specify in a direct manner the dissipated wave energy participating in the breaking process.

Noise emission under the extremely high intensity of the breaking process was investigated by Klusek and Lisimenka (2013) in the Large Wave Flume, GWK LUH (Leibniz University, Hannover). Energies of wave trains were larger by several orders of magnitude than in other experiments. It was rather surprising that the values of conversion between the two forms of energy were rather low, below 10^{-8}, in contrast to those reported in other experimental patterns, in particular, the increasing efficiency of energy conversion with the intensity of breaking.

It should be noted that the dispersion of outcomes regarding energy transformation would issue from incompatibilities in physicochemical parameters of medium and methods of simulation. Besides, the class of acoustic source models used in processing would have an effect on noise computation, because authors proceed by assuming, not always rightly, that the noise source has the character of a near-surface acoustic dipole. This is despite the fact that recording was performed in the near zone of an extended bubble cloud. In some field observations, sound data would likely contain input from other than solitary local sources.

The most striking outcome of a comparative analysis of all experiments is that in individual experiments, values of fraction of converted forms of energy tend to increase with the intensity of breaking. However, the results of separate experiments performed with different wave energies do not follow a specific pattern, which requires a separate exploration.

5. Conclusions

Based on a physical model aimed at clarifying the connections between the wave energy dissipation in the two breaking regimes and the emitted acoustic energy, the experiments were performed and the relationships parametrised.

The motivation for this investigation is the large scattering of values in the fraction of the dissipated wave energy's conversion into the energy of the emitted noise.

The experiments were performed using plunging and spilling wave packets with the pre-breaking energy of the plungers within a range of about 150 J to 300 J — an energy range in which this type of experiment has yet to be conducted.

In order to avoid the uncertainty due to multiple sound reflections in the channel and the impact of the cut-off propagation phenomenon on the recorded noise, modelling of sound propagation in the flume was applied. This approach used a relatively standard model of sound propagation in waveguides, not taking into account both the multiple scattering inside the bubble cloud and attenuation by bubbles. Within the frequency range around the cut-off frequency for this waveguide, corrections of the spectrum level on the basis of the model of images were used in order to calculate the total noise energy.

Having been corrected, the characteristic pattern of the noise spectral parameter of the spectral slope is in a frequency range of 1—12.5 kHz, and thus comparable to the case of the wind-driven noise spectra observed in the ocean, i.e. −5 to −6 dB/octave.

The effectiveness of the conversion of wave energy dissipated in the breaking to acoustic energy increases with the breaking intensity. It was also established that the rate of the dissipation coefficient is diminishing in the course of increasing the pre-breaking energy of wave packets.

Due to the simultaneous recordings of noise at several points along the breaking area, the hypothesis of a higher level of noise in the direction of propagation wave packets, in relation to the area behind the breaking wave, was demonstrated.

In particular, we emphasised that the ratio of conversion of the dissipated wave energy into acoustic is in the order of 10^{-8}, which confirms the outcome of several earlier investigations into higher intensity breaking events.

It may be hoped that these findings may inspire the further development of passive acoustic methods as the most appropriate for determining the dissipation of wave energy during breaking at sea.

Especially interesting for future investigations would be low energetic spillers, for which the wave's dissipation coefficient is still rather poorly correlated with the wave packet energy.

Acknowledgements

These results have been achieved thanks to financing within the framework of the grant “Experimental studies on dependence on energy dissipation of breaking waves and acoustic noise generated during process of breaking”, No. 2011/03/B/ST10/05977 by the National Science Centre of Poland.

References

Allen, J.B., Berkley, D.A., 1979. Image method for efficiently simulating small-room acoustics. J. Acoust. Soc. Am. 65 (4), 943—950, http://dx.doi.org/10.1121/1.382599.

Anguelova, M.D., Huq, P., 2018. Effects of salinity on bubble cloud characteristics. J. Mar. Sci. Eng. 6 (1), art. no. 1, http://dx.doi.org/10.3390/jmse6010001.

Bass, S.J., Hay, A.E., 1997. Ambient noise in the natural surf zone: wave breaking frequencies. In: IEEE OCEANS '98 Conference Proceedings. 1373—1377, http://dx.doi.org/10.1109/OCEANS.1998.726293.

Blenkinsopp, C.E., Chaplin, J.R., 2007. Void fraction measurements in breaking waves. Proc. Roy. Soc. A 463, 3151—3170, http://dx.doi.org/10.1098/rspa.2007.1901.

Blenkinsopp, C.E., Chaplin, J.R., 2011. Void fraction measurements and scale effects in breaking waves in freshwater and seawater. Coast. Eng. 58, 417—428, http://dx.doi.org/10.1016/j.coastaleng.2010.12.006.

Brekhovskikh, L.M., Godin, O.A., 1990. Acoustic of Layered Media, Part I. Springer-Verlag, 240 pp.

Carey, W.M., Browning, D., 1988. Low-frequency ocean ambient noise: measurements and theory. In: Kerman, B.R. (Ed.), Natural Mechanisms of Surface-Generated Noise in the Ocean. Reidel, Dordrecht, 361—376, http://dx.doi.org/10.1007/978-94-009-3017-9_26.

Carey, W.M., Fitzgerald, J.W., 1993. Low frequency noise from breaking waves. In: Kerman, B.R. (Ed.), Natural Physical Sources of Underwater Sound. Springer, Dordrecht, 277—304, http://dx.doi.org/10.1007/978-94-011-1626-822.

Carey, W.M., Fitzgerald, J.M., Monahan, E.C., Wang, Q., 1993. Measurement of the sound produced by a tipping through with fresh and salt water. J. Acoust. Soc. Am. 93, 3178—3192, http://dx.doi.org/10.1121/1.405702.

Cartmill, J.W., Su, M.Y., 1993. Bubble size distribution under saltwater and freshwater breaking waves. Dynam. Atmos. Oceans 20, 25—31, http://dx.doi.org/10.1016/0377-0265(93)90046-A.

Chanson, H., Aoki, S., Hoque, A., 2006. Bubble entrainment and dispersion in plunging jet flows: freshwater versus seawater. J. Coastal Res. 22 (3), 664—677, http://dx.doi.org/10.2112/03-0112.1.

Dean, R.G., Dalrymple, R.A., 1984. Water Wave Mechanics for Engineers and Scientists. World Scientific, Singapore, 353 pp.

Deane, G.B., 1999. Acoustic hot-spots and breaking wave noise in the surf zone. J. Acoust. Soc. Am. 105 (6), 3151—3167, http://dx.doi.org/10.1121/1.424646.

Deane, G.B., Stokes, M.D., 2010. Model calculations of the underwater noise of breaking waves and comparison with experiment. J. Acoust. Soc. Am. 127 (6), 3394—3410, http://dx.doi.org/10.1121/1.3419774.

Gibbs, B.M., Jones, K., 1972. A simple image method for calculating the distribution of sound pressure levels within an enclosure. Acta Acust. United Ac. 26, 24—32.

Goda, Y., 2000. Random Seas and Design of Maritime Structures. World Scientific, Singapore, http://dx.doi.org/10.1142/3587.

Haines, M.A., Johnson, B.D., 1995. Injected bubble populations in seawater and fresh water measured by a photographic method. J. Geophys. Res. 100, 7057—7068, http://dx.doi.org/10.1029/94JC03226.

Hollett, R.D., 1994. Observations of underwater sound at frequencies below 1500 Hz from breaking waves at sea. J. Acoust. Soc. Am. 95, 165—170, http://dx.doi.org/10.1121/1.408374.

Ingard, U., 1951. On the reflection of a spherical sound wave from an infinite plane. J. Acoust. Soc. Am. 23, 329—335, http://dx.doi.org/10.1121/1.1906767.

Kennedy, R.M., 1992. Sea surface sound dipole source dependence on wave-breaking variables. J. Acoust. Soc. Am. 91 (4), 1974—1982, http://dx.doi.org/10.1121/1.403681.

Kennedy, R.M., 1993. Acoustic radiation due to surface wave breaking. J. Acoust. Soc. Am. 94 (4), 2443—2445, http://dx.doi.org/10.1121/1.407466.

Kerman, B.R., 1984. Underwater sound generation by breaking wind waves. J. Acoust. Soc. Am. 75 (1), 149—165, http://dx.doi.org/10.1121/1.390409.

Klusek, Z., Lisimenka, A., 2007. Ambient sea noise in the Baltic Sea. In: Proceed. of the 2nd Intern. Conf. & Exhibition on Underwater Acoustic Measurements: Technologies & Results, Heraklion, Crete, 625—634.

Klusek, Z., Lisimenka, A., 2013. Acoustic noise generation under plunging breaking waves. Oceanologia 55 (4), 809—836, http://dx.doi.org/10.5697/oc.55-4.809.

Kolaini, A.R., 1998. Sound radiation by various types of laboratory breaking waves in fresh and salt water. J. Acoust. Soc. Am. 103 (1), 300—308, http://dx.doi.org/10.1121/1.421115.

Kolaini, A.R., Crum, L.A., 1994. Observations of underwater sound from laboratory breaking waves and the implications concerning ambient noise in the ocean. J. Acoust. Soc. Am. 96 (3), 1755—1765, http://dx.doi.org/10.1121/1.410254.

Kolaini, A.R., Roy, A., Gardner, D.L., 1994. Low-frequency acoustic emissions in fresh and salt water. J. Acoust. Soc. Am. 96 (3), 1766—1772, http://dx.doi.org/10.1121/1.411323.

Lamarre, E., Melville, W.K., 1991. Air entrainment and dissipation in breaking waves. Nature 351, 469—472, http://dx.doi.org/10.1038/351469a0.

Li, D., Farmer, D., 1993. Passive acoustical measurements of scale, probability, and intensity of wave breaking. In: IEEE Proceedings of OCEANS '93 Engineering in Harmony with Ocean, vol. 2, 193—197, http://dxdoi.org/10.1109/OCEANS.1993.326090.

Li, D., Farmer, D., 1994. Observations of breaking surface wave statistics. J. Phys. Oceanogr. 24, 1368—1387, http://dx.doi.org/10.1175/1520-0485(1994)024<1368:OOBSWS>2.0.CO;2.

Loewen, M.R., Melville, W.K., 1994. An experimental investigation of the collective oscillations of bubble plumes entrained by breaking waves. J. Acoust. Soc. Am. 95 (3), 1329—1343, http://dx.doi.org/10.1121/1.408573.

Means, S.L., Heitmeyer, R.M., 2001. Low-frequency sound generation by an individual open-ocean breaking wave. J. Acoust. Soc. Am. 110, 761—767, http://dx.doi.org/10.1121/1.1379729.

Means, S.L., Heitmeyer, R.M., 2002. Surf-generated noise signatures: a comparison of plunging and spilling breakers. J. Acoust. Soc. Am. 112 (2), 481—489, http://dx.doi.org/10.1121/1.1491256.

Medwin, H., Daniel, A.C., 1990. Acoustical measurements of bubble production by spilling breakers. J. Acoust. Soc. Am. 88 (1), 408—412, http://dx.doi.org/10.1121/1.399917.

Melville, W.K., Loewen, M., Felizardo, F., Jessup, A., Buckingham, M., 1988. Acoustic and microwave signatures of breaking waves. Nature 336, 53—56.

Melville, W.K., Loewen, M.R., Lamarre, E., 1993. Bubbles, noise and breaking waves: a review of laboratory experiments. In: Kerman, B.R. (Ed.), Natural Physical Sources of Underwater Sound. Kluwer Acad. Publ., 483—501, http://dx.doi.org/ 10.1007/978-94-011-1626-8_36.

Orris, G.J., Nicholas, M., 2000. Collective oscillations of fresh and salt water bubble plumes. J. Acoust. Soc. Am. 107 (2), 771—787, http://dx.doi.org/10.1121/1.428253.

Paprota, M., 2017. Experimental study on wave-current structure around a pneumatic breakwater. J. Hydro-Environ. Res. 17, 8—17, http://dx.doi.org/10.1016/j.jher.2017.09.002.

Prosperetti, A., 1988. Bubble-related ambient noise in the ocean. J. Acoust. Soc. Am. 84 (3), 1042—1054, http://dx.doi.org/10.1121/1.396740.

Slauenwhite, D.E., Johnson, B.D., 1999. Bubble shattering: differences in bubble formation in fresh water and seawater. J. Geophys. Res. 104 (C2), 3265—3275, http://dx.doi.org/10.1029/1998JC900064.

Szuszkiewicz, J., Klusek, Z., 2018. Underwater noise emitted during small-scale air entrainment events. Oceanol. Hydrobiol. Stud. 47 (1), 87—97, http://dx.doi.org/10.1515/ohs-2018-0010.

Tęgowski, J., 2004. A laboratory study of breaking waves. Oceanologia 46 (3), 365—382.

Wu, J., 2000. Bubbles produced by breaking waves in fresh and salt waters. J. Phys. Oceanogr. 30 (7), 1809—1813, https://doi.org/10.1175/1520-0485(2000)030<1809:BPBBWI>2.0.CO;2.